Deubiquitinase USP9X loss Sensitizes Cancer Cells to mTOR Inhibitors through p62 Dysregulation

Juan M. Roldán-Romero
Spanish National Cancer Research Centre: Centro Nacional de Investigaciones Oncologicas
Maria Santos
Spanish National Cancer Research Centre: Centro Nacional de Investigaciones Oncologicas
Javier Lanillos
Spanish National Cancer Research Centre: Centro Nacional de Investigaciones Oncologicas
Pablo Maroto
Hospital de la Santa Creu i Sant Pau
Georgia Anguera
Hospital de la Santa Creu i Sant Pau
Bruna Calsina
Spanish National Cancer Research Centre: Centro Nacional de Investigaciones Oncologicas
Angel Martinez-Montes
Spanish National Cancer Research Centre: Centro Nacional de Investigaciones Oncologicas
María Monteagudo
Spanish National Cancer Research Centre: Centro Nacional de Investigaciones Oncologicas
Sara Mellid
Spanish National Cancer Research Centre: Centro Nacional de Investigaciones Oncologicas
Luis J. Leandro-García
Spanish National Cancer Research Centre: Centro Nacional de Investigaciones Oncologicas
Cristina Montero-Conde
Spanish National Cancer Research Centre: Centro Nacional de Investigaciones Oncologicas
Alberto Cascón
Spanish National Cancer Research Centre: Centro Nacional de Investigaciones Oncologicas
Giovanna Roncador
Spanish National Cancer Research Centre: Centro Nacional de Investigaciones Oncologicas
Javier Coloma
Spanish National Cancer Research Centre: Centro Nacional de Investigaciones Oncologicas
Mercedes Robledo
Spanish National Cancer Research Centre: Centro Nacional de Investigaciones Oncologicas
Cristina Rodriguez-Antona (crodriguez@cnio.es)
Spanish National Cancer Research Centre: Centro Nacional de Investigaciones Oncologicas

Research

Keywords: mTOR inhibitors, renal cell carcinoma, USP9X, ubiquitination, sequestosome

Posted Date: September 28th, 2021

DOI: https://doi.org/10.21203/rs.3.rs-923880/v1

Abstract

Background

Mutations in *MTOR* and *TSC1/2* can only explain part of variability in mTOR inhibitor response. Here, we performed a comprehensive molecular characterization of tumors with high sensitivity to these drugs to uncover novel mechanisms of response.

Methods

Chromophobe renal cell carcinoma (chRCC) tumors were analyzed by whole-exome sequencing. Rapamycin sensitivity, expression of mTOR pathway effectors, ubiquitylome analyses to identify USP9X substrates, p62 immunoprecipitation and autophagy assessment through immunofluorescence assays for p62 and LC3 were performed in USP9X depleted HeLa and 786-O cells for mechanistic investigation.

Results

Whole-exome sequencing of chRCC patients with high mTOR inhibitor sensitivity, uncovered USP9X deubiquitinase as the only mutated gene shared by these tumors. The clonal characteristics of the mutations, revealed by studying multiple primary and metastatic samples, together with the low *USP9X* mutation rate in unselected chRCC series, implied a causal link between *USP9X* and mTOR inhibitor sensitivity. The high sensitivity was recapitulated *in vitro*, and while no direct effect on mTORC1 was detected, an unbiased ubiquitylome analysis revealed p62 as a direct USP9X target. Bortezomib treatment, which also led to p62 ubiquitination, increased rapamycin effect. Finally, immunofluorescence assays for p62 and LC3 confirmed dysregulated autophagy in USP9X depleted cells, supporting a synthetic lethal interaction between rapamycin-induced autophagy via mTOR-axis and USP9X loss.

Conclusions

Our study uncovers USP9X as a potential novel marker of sensitivity to mTOR inhibitors and suggests the inhibition of this gene as a clinically exploitable strategy able to increase sensitivity to these drugs through a novel p62 regulatory mechanism.

Background

mTOR pathway has a central role in cell biology as it coordinates nutrients with metabolic activity and cell division. Its over-activation is a frequent event in cancer, with point mutations in *MTOR, TSC1* and *TSC2* present in 6% of the tumors in the Pan-Cancer project and *MTOR* amplification in 4% of tumors (1). Two mTOR pathway inhibitors, temsirolimus and everolimus, are approved for the treatment of renal cell carcinoma, progressive pancreatic neuroendocrine tumors, subependymal giant cell astrocytoma associated with tuberous sclerosis complex and HER2-negative breast cancer.

There is large variability in the response to mTOR inhibitors. Extraordinary responses have been linked to specific mutations in *MTOR, TSC1* and *TSC2* that by over-activation of the pathway result in increased rapalog sensitivity (2–7). However, studies on large series of treated patients found an incomplete correlation between these alterations and mTOR inhibitor response (8–11). Intra-tumor heterogeneity may explain part of this discordance, with extraordinary responses being driven by early mutations in these genes or by parallel evolution in different tumor subclones, leading in both cases to a high mTOR pathway dependency in all tumor cells (5, 12, 13). In addition, cases without mTOR pathway mutations and high sensitivity to mTOR inhibitors suggest a role for still unidentified genes, which would represent novel predictive markers and potential drug targets in cancer.

In this study, by applying whole exome sequencing (WES) to three chromophobe renal cell carcinoma (chRCC) patients with high sensitivity to temsirolimus, we discovered *USP9X* as the only mutated gene shared by the tumors. This deubiquitinase was found rarely mutated in unselected chRCC cases and *in vitro* cellular models validated the association with mTOR inhibitor sensitivity. Ubiquitylome studies revealed p62 as a USP9X substrate and ubiquitination of this protein was identified as a pivotal postranscriptional modification involved in autophagy regulation, supporting a synthetic lethal interaction between USP9X and mTOR inhibitors.

Methods

Patients

Three metastatic chRCC patients with high sensitivity to temsirolimus treatment were selected for WES. In brief, patient 1 was a 34-year old woman with metastatic chRCC at diagnosis. She received temsirolimus which resulted in complete response in all metastatic lesions and 80% decrease of the renal tumor volume, with the remaining tumor removed by nephrectomy. The patient received again temsirolimus for a bone metastasis detected 9 years after the initial diagnosis. Again a complete response was obtained and, currently, 13 years after the initial diagnosis the patient is disease free. The response to the first temsirolimus treatment has been published (4). Patient 2 was a 49-year old man with a localized chRCC removed by surgery that 15 years later developed a retrovesical/ perirectal metastasis and started temsirolimus treatment. Maintained radiological response was observed by MRI and after 23 months the patient stopped treatment, underwent surgery and was disease free for 52 months. At this point, metastatic lesions were detected, and the patient received temsirolimus again for 1 year obtaining response. 20 months after stopping temsirolimus, metastases were again detected, removed by surgery and currently monitoring of the patient continues. Patient 3 was a 68-year old woman with a stage III chRCC that 3.5 years after the nephrectomy developed multiple lymph node metastases. Temsirolimus treatment achieved a 35% reduction in tumor size, but 1 year later treatment was stopped due to toxicity with a maintained response of 11 months after stopping temsirolimus. A detailed description of these three patients is provided in Supplementary Methods. Tumor mutations in genes frequently altered in chRCC and immunohistochemistry characteristics for these three cases and a large series of 89 chRCC patients, was recently published by our group (14).

The study was approved by the Instituto de Salud Carlos III Review Board, and the patients provided written informed consent to participate in the study.

Whole exome sequencing (WES)

WES analysis was performed in the three patients: in blood and in available FFPE tumors blocks with sufficient material (e.g. some biopsies were excluded; Fig. S1). DNA was extracted from the tumor tissues using the Maxwell® RSC DNA FFPE Kit (Promega) and the Maxwell® RSC Instrument (Promega). Samples with highly degraded DNA unsuitable for library production were excluded. DNA from peripheral blood was isolated using DNeasy Blood and Tissue Kit (Qiagen) according to the manufacturer instructions.

DNA libraries were produced using the SureSelect XT HumanAllExon V5 kit (Agilent Technologies), and sequencing was performed in a HiSeq instrument (Illumina) using a 100-bp paired-end mode. WES mean depth of coverage was > 90x for all samples. Raw sequencing data was aligned to hs37d5 (GRCh37) reference genome using BWA-mem. Somatic variant calling of the tumor with germline-matched samples was performed using Mutect (GATK v3.4). Sequencing data was analyzed to identify single nucleotide variants (SNVs) and small insertions or deletions (indels), applying an allele frequency threshold of 0.10 and with ≥ 2 alternative reads supporting the variant. Those variants present in gnomAD (https://gnomad.broadinstitute.org/) with an allele frequency > 0.0001 were not considered further. Coding non-synonymous and loss-of-function variants (labelled as Moderate or High Impact by VEP; e.g. missense, nonsense, those disrupting canonical splice sites, in-frame and frameshift indels), were retained for the analysis, as previously described (4).

Immunohistochemistry (IHC)

USP9X IHC was performed on tumor tissue sections using ab180191 antibody (Abcam), following standard protocols. The specificity of the antibody was confirmed using HAP1 *USP9X* knock-out (KO) and HAP1 wild type cells (Horizon Discovery).

Cell lines and culture

Cell line authentication for HeLa and 786-O cell lines was performed using the GenePrint® 10 kit (Promega) and cells were verified to be free of mycoplasma (MTC-NI System; Millipore). HeLa and 786-O cells were grown with high glucose DMEM with L-glutamine (Sigma) supplemented with 10% FBS. For serum starvation, cells were washed three times with PBS and incubated with culture media without FBS for 16 h. For serum plus amino acid starvation, after the 16 h without FBS, cells were washed and incubated with PBS for 1h. For stimulation experiments, starved cells were incubated with media with FBS (20%) and amino acids for 30 min. Cell proteins were extracted and used for immunoblotting (methods and antibodies are described in detail in Suppl. Methods).

USP9X **gene silencing**

USP9X shRNA-mediated gene knock-down was performed using pTRIPZ human *USP9X* doxycycline inducible vectors containing 4 different shRNAs (RHS4740-EG8239; clone ID: V2THS41519; V2THS41521; V3THS320834; V2THS41523; these were referred to in the text as #1, #2, #3 and #4, respectively) and a non-target shRNA (Dharmacon). Lentiviral infections were performed according to the manufacturer's instructions. After puromycin selection, cells were grown with doxycycline at 1 µg/ml to induce shRNA expression and silence *USP9X*. After protein isolation of the different shRNA transduced cells and western-blot, V2THS41523 (#4) was discarded due to poor *USP9X* silencing.

USP9X-KO cells were generated with the CRISPR/Cas9 system. CRISPR guide sequences targeting exon 3 of the human *USP9X* gene (5′-CATACTGACTTGGCCAAGTT-3′ and 5′-AGTTGGATGACATGATCAAC-3′) were designed using the Cas9-Designer, optimized using Cas-OFFinder, and cloned into lentiviral plasmids. SpCas9 expression plasmids (500 ng) and sgRNA plasmids (500 ng) were transfected into 2×10^5 HEK293T cells using Lipofectamine 2000 (Thermofisher). Lentiviral particles were used to transduce HeLa and 786-O cell lines. After 10 days of growth in media with puromycin, cells were diluted and sorted to establish single-cell clones. Proteins were isolated from each single colony and *USP9X* KO cells identified by western-blot. Mutations in the *USP9X* target region were analyzed by Sanger sequencing.

MTT viability assays

Cells were seeded in 96-well plates at 1250 (HeLa) or 2000 (786-O) cells per well and after 8 h treated with rapamycin, WP1130, bortezomib, or a combination of drugs, at different concentrations for 32–96 h, depending on the cell type and compound tested. Eight replicates for each concentration were used with a 1% DMSO final concentration, in at least two independent plates. For shRNA experiments, doxycycline was added to the media, at least 3 days before plating and during the MTT experiments. MTT solution was incubated at 1g/l for 2 h at 37ºC, media was removed and cells lysed with DMSO. Compounds were added to the plates using the Biomeck NP^X Laboratory Automation Workstation (Beckman Coulter). Absorbance at 544 nm was assessed with a microplate reader (VICTOR Multilabel Plate Reader; PerkinElmer).

K-ε-GG profiling and proteome analysis

Cellular pellets were lysed in 5% SDC, 100 mM TrisHCl buffer pH 7.5, supplemented with protease and phosphatase inhibitors (HALT, Pierce) and Benzonase (Merck). Proteins were reduced and alkylated 1 h at room temperature with 15 mM TCEP and 35 mM 2-chloroacetamide (Sigma). Lysates were then digested with Lys-C (Wako, enzyme/ protein ratio 1:200) followed by trypsin (Trypzean, Sigma; enzyme/ protein ratio 1:50). Digests were quenched with TFA, peptides desalted and lyophilized. For enrichment of K-ε-GG peptides, the PTMScan ubiquitin remnant motif (K-ε-GG) kit (Cell Signaling Technology, 5562) was used. Eluted peptides were desalted using StageTips and analyzed by coupling an UltiMate 3000 RSLCnano LC system to a Q Exactive Plus mass spectrometer (Thermo Fisher Scientific). Raw files were processed with MaxQuant (v 1.6.1.0) using the standard settings against a human protein database (UniProtKB/TrEMBL, 20,303 sequences, march 2018) supplemented with common found laboratory contaminant protein

sequences. Carbamidomethylation of cysteines was set as a fixed modification whereas oxidation of methionines, protein N-term and addition of glycine-glycine to lysine (K-GG) as variable modifications. Results were filtered at 0.01 FDR (peptide and protein level). For label free quantification match between runs option was enabled. Afterwards, the “GlyGly (K)Sites.txt” file was loaded in Prostar (v1.10) (15) using the intensity values for further statistical analysis. A global normalization of log2-transformed intensities across samples was performed using the median. Missing values were imputed using the algorithms imp4p (for partially observed values) and Lapala (for values missing on an entire condition). Differential analysis was done using the empirical bayes statistics limma. The FDR was estimated using Benjamini-Hochberg procedure.

p62 transfections and structural model of p62-UBA and ubiquitin

Cells were seeded into 96-well plates and once attached, transfected in the same plate with p62-wildtype (HA-p62, Addgene plasmid #28027) or p62-K435R using Lipofectamine 2000 (ThermoFisher Scientific). After transfection, medium was replaced and 58 h later MTT was used to measure cell viability.

For the structural representation of p62 K435, the structure of the UBA domain obtained by NMR was used (PDB code: 2knv). Model 1 from the ensemble was used as a representative structure for visualization purposes. The structure of ubiquitin (PDB code: 1ubq) was visualized at the same scale as p62 UBA domain using the program Coot (16). The surface of ubiquitin was computed using the program PyMOL (17).

p62 immunofluorescence quantification

Cells cultured in 96 well plates were fixed with 4% paraformaldehyde in PBS at room temperature and permeabilized with 0.2% Triton X-100 in PBS for 5 min. After washing three times with PBS, cells were incubated with blocking buffer (1% BSA in PBS) at 37ºC for 30 min. Then, blocking buffer was removed and were incubated with primary antibody at 1:100 dilution in blocking buffer (1% BSA in PBS) at room temperature for 1 h at 37ºC. Cells were then washed three times with PBS and incubated with Invitrogen's Alexa-conjugated secondary antibody at 37ºC for 30 min. Then, cells were washed 3 times with PBS and counterstaining of nuclei with 4,6-diamidino-2-phenylindole (DAPI).

Autophagy measurement using the DsRed-LC3-GFP reporter

Autophagy activity quantification was performed using a dual color fluorescent protein-tagged LC3 reporter as previously described (18). Retroviral plasmid containing cDNA dual color reporter was packed in retroviral vector and cells were transduced for 24 h followed by a selection with G418. After seven days of selection, high dsRed intensity cells were sorted to get a homogeneous population. Sorted cells were plated in 96 well plates, incubated for 24–32 h with rapamycin, chloroquine or DMSO, fixed in PFA 4% and analyzed by confocal microscopy with a Leica TCS SP5 Confocal Microscope. Quantification of cell size, number, size and intensity of dsRed positive vesicles per cell were performed using Definiens software.

Results

USP9X is the only mutated gene shared by three chRCC temsirolimus-responder patients

We performed WES on tumor and blood samples from three chRCC patients with high temsirolimus sensitivity, and annotated the number of somatic variants (present in the tumor and absent in the germline) leading to non-synonymous or loss-of-function variants. Figure 1 shows the number of mutated genes detected in the tumors from each patient (367, 33 and 37; also Table S1). Among all these mutated genes, 22 were involved in cancer, according to the Cancer Gene Census (e.g. *ATM, ERCC2, FANCD2, SPEN, TP53*), and only one (*TSC2*) in mTOR pathway regulation. Specifically, patient 1 carried two *TSC2* mutations detected at low frequency (c.5069-1G > C and c.3200_3201delinsAA, p.V1067E), as previously described (4).

We then identified mutated genes shared among the different tumors and found that only one (*USP9X*) was mutated in the three tumors, while seven genes were mutated in two tumors (*CDRT1, FANCD2, MMP2, MUC21, PRB2, SIPA1L3, TP53*, Fig. 1A). The mutations in *USP9X*, a gene located in the X chromosome, in patients 2 and 3 were loss-of-function (a nonsense mutation leading to p.Q2004* and a splicing site mutation c.3977 + 1G > T), and patient 1 had a missense mutation (c.4401A > G, p.I1467M) predicted as possibly pathogenic by Polyphen2 and damaging by SIFT. Sanger sequencing confirmed the presence of these mutations in the tumors (Fig. 1B) and absence in the peripheral blood of the patients (not shown).

IHC revealed that the two tumors with loss-of-function mutations lacked USP9X protein expression while, as expected, USP9X protein was detected in the tumor with the misssense variant (Fig. 1C). IHC in all available tumor tissues from patients 2 and 3 revealed a uniform lack of USP9X expression in all cancer cells along time (diagnostic biopsies, primary tumors and metastases, before and after treatment; see Fig. S1), indicating that *USP9X* mutations were early events during the evolution of these tumors. Since IHC was not informative to detect the somatic *USP9X* missense mutation in patient 1, we analyzed its presence by Sanger sequencing and NGS in all the tumor samples available. Patient 1 *USP9X* mutation had a similar allele frequency in all samples tested, from treatment naïve and post-treatment primary tumor to metastases in lymph nodes and bone, and it was similar to *TSC2* mutation frequency (Fig. S2).

USP9X mutations in cancer

To study *USP9X* mutational prevalence in chRCC, we collected 89 additional tumors enriched in metastatic cases (14). All these tumors showed a positive USP9X IHC staining and 3 of 84 cases with mutation data (3.6%) carried a *USP9X* missense mutation. These three patients had localized disease and did not receive systemic treatment. A comparison of the clinical characteristics of the *USP9X*-mutated and wild type patients did not reveal statistically significant differences in stage, metastatic status nor survival of the patients. Clinical details, together with the mutational landscape and IHC characteristics of this chRCC series was recently published(14). In the TCGA chRCC series, 2 of 65 tumors (3.0%) were mutated in *USP9X* with a missense and a frameshift variant (Fig S3).

Regarding other neoplasia, among the 32 different tumor types from the TCGA Pan-Cancer Atlas study, *USP9X* mutations were found in 392 of 10953 patients (3.5%), with the most frequent mutation types being missense and truncating variants (75% and 24%, respectively, Fig. S3). In the Pan-Cancer series, the highest rates of *USP9X* mutations correspond to uterine corpus endometrial carcinoma (16%), skin cutaneous melanoma (12%) and colorectal adenocarcinoma (6,5%).

USP9X depletion increases sensitivity to rapamycin

To investigate whether *USP9X* loss increases sensitivity to mTOR inhibitors, we depleted USP9X protein in HeLa cells through an inducible system using 3 different shRNAs. We also generated a renal cancer cell line model in the renal cancer 786-O cells through CRISPR/Cas9 strategy and confirmed that 3 clones with null USP9X protein expression had biallelic frameshift mutations in *USP9X.* Treatment of the cells with rapamycin resulted in decreased cell viability in the USP9X depleted cells, with a similar effect in both HeLa and 786-O cells (Fig. 2A and 2B). We also treated wild type cells with WP1130, a partially selective deubiquitinase inhibitor directly inhibiting USP9X, USP24 and UCH37 that has shown potent antitumor activity against a variety of cancers (19–21). Combining rapamycin with WP1130, decreased cell viability by a greater extent than each of the treatments alone (Fig. 2C and 2D). These data support that *USP9X* mutations cause the increased temsirolimus sensitivity observed in the patients.

To gain additional knowledge regarding the mechanism linking USP9X and mTOR inhibitors, western-blot analyses evaluating the activity of mTOR pathway in the USP9X-depleted HeLa and 786-O cells were performed. However, no significant changes in the central effectors of the pathway were detected (Fig. S4 shows HeLa results in normal growth conditions, starvation and stimulation). These results suggest that the increased rapalog sensitivity observed in cells lacking USP9X, might not be caused by a direct effect in the core mTOR pathway components, but rather to a downstream convergence that leads to a synthetic lethal interaction.

Ubiquitylome analysis detects p62 as a USP9X substrate

The deubiquitinase USP9X has been reported as a ubiquitous protein, with multiple substrates involved in a wide variety of functions. Thus, to identify potential substrates of USP9X that may be involved in the sensitization to rapamycin, we analyzed global ubiquitin changes caused by USP9X depletion. We used the PTMScan assay, a method based on an immunoprecipitation of ubiquitinated peptides with an antibody that recognizes the diglycine remnant left motif on ubiquitinated lysine residues after tryptic digestion (22), that allows to detect in an unbiased manner proteins with ubiquitin enrichment from the entire proteome of the cells. This approximation was applied to HeLa and 786-O cellular models, uncovering 164 and 91 ubiquitinated peptides with a statistically significant upregulation in USP9X depleted versus control cells, respectively (Fig. S5). Combined HeLa and 786-O analysis showed a group of thirteen peptides with a significant increased ubiquitination in both cell lines (Fig. 3A). Among these, SQSTM1/p62 (from hereon p62) had more than one enriched peptide distributed in HeLa and 786-O. Specifically, lysines 13, 157 and 435 in 786-O cells and lysines 264, 295, 313 and 435 in HeLa cells, were residues with increased ubiquitination (Fig. 3B). Importantly, K435 ubiquitination, shared by both cell

lines, was also overrepresented in a melanoma cell line silenced for *USP9X* (23), supporting that p62 polyubiquitination occurs upon USP9X depletion in diverse cancer cell models (Table S2). Furthermore, K435 is located in p62 UBA domain has been shown to regulate p62-mediated autophagy (24). In fact, transfection of USP9X-KO cells with a p62 K435 mutated construct altered cell growth (Fig. 3C) and a structural analysis of the UBA domain indicates that K435 ubiquitination could alter dimer formation and consequently p62 activity because of steric clashes between the ubiquitin molecules (Fig. 3D). Additionally, the bond formation between K435 and ubiquitin would remove the lysine charge which has been proposed to negatively impact p62 dimerization (25).

Proteasomal inhibition increases p62 polyubiquitination and sensitivity to rapamycin

To validate that ubiquitinated p62 was increased in USP9X depleted cells, we performed p62 immunoprecipitation and tested the molecular weight of the immunoprecipitated proteins (Fig. 4A). Bands with higher molecular weight were detected with p62 antibody in USP9X depleted cells, suggesting high levels of polyubiquitinated p62.

Proteasomal inhibition by bortezomib causes ubiquitin accumulation in a wide range of intracellular proteins including p62, which is found extensively ubiquitinated in several residues upon treatment with this drug (24, 26). We hypothesized that bortezomib-induced polyubiquitination could recapitulate the increased rapamycin sensitivity of the USP9X KO cells. In fact, in a hepatocellular cellular model, a combination of rapamycin with bortezomib has been shown to decrease cells viability further than these drugs alone (27). A global increase in total ubiquitin conjugate levels were observed in HeLa and 786-O wild type cells after incubation with bortezomib alone or in combination with rapamycin, while no effect was detected with rapamycin alone. Interestingly, a higher molecular weight p62 band was detected upon bortezomib-induced accumulation of ubiquitinated proteins, in agreement with previous studies reporting p62 ubiquitination in these conditions (Fig. 4B). Furthermore, treatment of HeLa and 786-O cells with bortezomib, significantly increased the sensitivity to rapamycin (Fig. 4C and 4D).

Depletion of USP9X leads to altered p62 foci and deregulation of autophagosome formation

p62 ubiquitination has been shown to regulate its dimerization and cargo-acceptor function during autophagy (24, 28). To assess the effect of *USP9X* loss in p62 function, we characterized p62 status *in vitro* by immunofluorescence (Fig. 5A). Notably, in basal conditions HeLa and 786-O USP9X depleted cells displayed higher numbers and larger size p62-positive-foci with less intensity than wild type cells (Fig. 5B), supporting that p62 cluster formation, a key step towards encapsulation of cargo-ubiquitinated proteins in autophagosomes, is altered in the absence of *USP9X*. Furthermore, upon treatment with rapamycin, p62-foci number and size increased, with greater effect in USP9X depleted cells (Fig. 5B). These differences augmented upon treatment with chloroquine, a well-known autophagy inhibitor that

impairs lysosome resolution, supporting autophagosome accumulation (29). Altogether, dynamic of p62-foci differed in *USP9X* KO and control cells, pointing to an alteration in p62 cluster formation.

Because rapamycin induces autophagy through mTOR inhibition, we determined whether USP9X depleted cells showed alterations in autophagy vesicles through the evaluation of the autophagosome marker LC3. We used the fluorescent protein-tagged LC3, formed by EGFP-LC3-dsRed in a retroviral expression plasmid, which allows to monitor autophagy activation and autophagosome formation as previously described by Sheen JH *et al* (18) (Fig. 5C). In basal conditions, no difference in the number of LC3-positive vesicles was observed between HeLa USP9X depleted and control cells (Fig. 5D). However, treatment with rapamycin or chloroquine significantly increased the number, size and intensity of autophagosomes in USP9X depleted cells. Thus, the increased LC3 puncta detected in *USP9X* KO cells upon rapamycin treatment, suggests that autophagy dysregulation underlies the increased mTOR inhibitor sensitivity observed in patients with *USP9X* mutations (30).

Discussion

By performing a genomic mutational screening of three chRCC patients highly sensitive to temsirolimus, we identified the deubiquitinase USP9X as the only somatically mutated gene shared among the patients. This served as the basis to discover a synthetic lethal interaction between USP9X and the mTOR pathway, directly implicating USP9X in the regulation of p62-mediated autophagy through ubiquitination, and resulting in tumor cell sensitization to mTOR inhibitors (Fig. S6).

USP9X is a ubiquitous and multifunction deubiquitinase involved in mitosis as a structural component of centrosomes (31, 32), in DNA repair (33), in ciliogenesis (34) and in lysosomal damage (35). Mutations in *USP9X* have been found in multiple tumor types at low frequency rate (36), with the highest proportion of mutations found in uterine tumors and melanoma. *USP9X* is mutated in 3% of unselected chRCC tumors, however, the three patients with a high mTOR inhibitor sensitivity described herein had mutated tumors, supporting an association between the mutation of this gene and treatment response.

Furthermore, USP9X depletion in cellular models increased rapamycin effect, recapitulating the therapeutic responses observed in the patients. In this regard, our cell models mimicked patients 2 and 3, with no mutations in mTOR pathway (e.g. in *MTOR, TSC1, TSC2*), while patient 1 carried one *USP9X* and two *TSC2* mutations in the tumor, with variant allele frequencies that remained unaltered in four different tumor lesions obtained along 9 years of disease (Fig. S2), suggesting early mutations during tumorigenesis. We previously showed that the *TSC2* mutations found in patient 1 conferred a tumor dependency on mTOR pathway (4), thus, the addition of a *USP9X* mutation would be expected to lead to a stronger synergistic effect with mTOR inhibition, explaining the exquisite sensitivity to temsirolimus observed in this patient. The crosstalk between USP9X and mTOR pathway was reinforced by the increased rapamycin sensitivity observed in cell lines treated with WP1130, a partly selective deubiquitinase inhibitor directly acting on USP9X, USP5, USP14 and UCH37 (37). Indeed, WP1130 has been shown to increase sensitivity to other drugs, including doxorubicin, cisplatin or gemcitabine (38–41)

and diverse mechanisms such as autophagy alteration, p53 downregulation, or induction of oxidative stress bulk, were proposed to mediate this effect.

Despite an initial study suggesting that USP9X was involved in mTOR pathway regulation through stabilization of Raptor under nutrient stimulation (42), we could not confirm this in HeLa and 786-O cells. Recently, Wrober *et al* reported Rictor as a potential substrate of USP9X and found reduced levels of Ser473-AKT phosphorylation when USP9X was transiently silenced through siRNA (43). However, another study found no effect on AKT using a similar USP9X depletion strategy in the same cell lines (44). In our study, we observed a small reduction of pAKT (Ser 473) levels in HeLa *USP9X* silenced cells (Fig. S4) upon stimulation and starving conditions. These differences in mTORC2 results suggest transient and cell line dependent effects. In contrast, USP9X-mediated autophagy dysregulation has been consistently observed in different cell lines with different strategies targeting USP9X, such as siRNA (43), CRISPR/Cas9 (this study) or pharmacological inhibition (38). In addition, we did not find proteins related with mTOR pathway in an unbiased ubiquitylome experiment directed to identify USP9X substrates. This analysis revealed USP9X-mediated multisite ubiquitination of p62, in agreement with previous analyses in a melanoma and HeLa cell lines (23, 44), and it was concordant with the higher molecular weight bands observed in USP9X depleted cells after p62 immunoprecipitation (Fig. 4A), frequently observed in conditions of p62 polyubiquitination (45). Posttranslational modifications in p62 have been described to alter its function as a protein adaptor and signaling hub. These modifications include phosphorylation at Ser403 and Ser349 (46, 47), proteolytic cleavage by Caspase 8 (48) and ubiquitination by NEDD4, TRIM21 and UBE2D2/UBE2D3 (24, 28, 49). Pan *et al* reported that ubiquitination of p62 in lysine 7 impaired protein sequestration (28) and Peng *et al* showed that multi-site ubiquitination of p62 regulated selective autophagy (24). Interestingly, acetylation at K420 and K435 has been shown to disrupt UBA dimerization and cause increased binding of p62 to ubiquitin (25), again supporting posttranslational modifications as important events regulating p62 function. Furthermore, bortezomib exerts a robust effect on p62 ubiquitination and a synergistic effect with rapamycin has been described in *in vitro* models (24, 27). Similarly, we found that bortezomib sensitized HeLa and 786-O cells to rapamycin. These results suggest that USP9X loss leads to a p62 dysregulation, with fatal consequences when converges with mTOR pathway inhibition.

Our p62 immunofluorescence analysis unveiled a broadening in number and size of p62 foci in USP9X depleted cells, potentially related with a dysregulation of p62 oligomerization, phase-condensation and/or aggregates formation, which are required for selective autophagy, in line with the large p62 bodies described in MEF *ATG5* KO cells, where autophagy is compromised (50). In agreement, the dsRed-LC3 vesicles analysis revealed that *USP9X* KO cells displayed higher number, size and intensity of autophagosomes, which would indicate autophagy dysregulation (30). The exacerbation of this effect by chloroquine, supports further LC3 accumulation in *USP9X*-KO cells. Similarly, Wrobel *et al* found that transient knock-down of *USP9X* reduced the levels of LC3-II with and without bafilomycin A1, consistent with an impairment of autophagosome formation (43).

Conclusion

In summary, our data suggests mTOR inhibitor treatment as a therapeutic opportunity for *USP9X* mutated tumors and underpins *USP9X* pharmacological inhibition as a novel strategy to increase tumor vulnerability to these agents. This study supports that the underlying mechanism for this enhanced sensitivity to mTOR inhibitors is a synthetic lethal interaction, mediated by the effect of USP9X on p62 ubiquitination and autophagy (Fig. 6). Therefore, this study reinforces a key role for the emerging field of posttranscriptional modifications in tumor drug response, and propose USP9X not only as a novel response marker, but also as a potential therapeutic target in cancer.

Abbreviations

chRCC
chromophobe renal cell carcinoma
indels
small insertions or deletions
KO
knock-out
SNVs
single nucleotide variants
WES
whole exome sequencing.

Declarations

Ethics approval and consent to participate

The study was approved by the Instituto de Salud Carlos III Review Board (CEI PI 46_2019-v2), and the patients provided written informed consent to participate in the study.

Consent for publication

Not applicable.

Availability of data and materials

All data generated or analysed during this study are included in this published article and its supplementary information files.

Competing interests

The authors declare that they have no competing interests

Funding

This work was supported by the projects RTI2018-095039-B-I00 (Spanish Ministry of Economy, Industry and Competitiveness MEIC/AEI, co-funded by the European Regional Development Fund ERDF), the “Club de Atletisme A 4 el KM” from Les Franqueses del Vallés (PM), Young SOGUG Fellowship, Spanish Oncology GenitoUrinary Group (GA), “La Caixa” Foundation (ID 100010434) Doctorate in Spain Fellowship Programme (LCF/BQ/DE16/11570014)(JMRR), “La Caixa” Foundation INPhINIT – Retaining Fellowship Programme (LCF/BQ/DR19/11740015) (JL) and the Spanish Ministry of Education, Culture and Sport "Formación del Profesorado Universitario - FPU" fellowship with ID number FPU2016/05527 (MS).

Authors’ contributions

Conceptualization and design of experiments: JMR-R, CR-A

Patient selection and acquisition of clinical samples and patients’ data: PM, GA

Performed bioinformatic analysis of NGS data: JL and AM-M

Performed genetic interpretation of data: JMR-R, MS, JL, AC, MR and CR-A

Performed and analyzed all in vitro experiments: JMR-R

Provided support to JMR-R for in vitro experiments: MS, BC, MM, SM, LJL-G, CM-C

Performed immunohistochemistry: GR

Performed Fig. 3D modeling: JC

Interpretation of experimental data: all authors

Writing of original draft: JMR-R, CR-A

Critical review of the manuscript: All authors

Acknowledgments

We thank CNIO Confocal Microscopy Unit for their support and expertise performing confocal microscopy analysis for dsRed and p62 immunofluorescence. Sergi Beltran and Sophia Derdak from CNAG for their support in whole-exome sequencing. Sandra Rodriguez-Perales and Raul Torres from CNIO Molecular Cytogenetics Unit for their support generating CRISPR/Cas9 knock-out cells. Fernando García and Javier Muñoz from CNIO Proteomics Unit for all their help and effort regarding ubiquitinome analysis. Nabil Djouder for discussions along the project and Sergio Ruiz-Llorente for technical support.

References

1. Zhang Y, Kwok-Shing Ng P, Kucherlapati M, Chen F, Liu Y, Tsang YH, et al. A Pan-Cancer Proteogenomic Atlas of PI3K/AKT/mTOR Pathway Alterations. Cancer Cell. 2017;31(6):820-32 e3.

2. Espinosa M, Roldan-Romero JM, Duran I, de Alava E, Apellaniz-Ruiz M, Cascon A, et al. Advanced sporadic renal epithelioid angiomyolipoma: case report of an extraordinary response to sirolimus linked to TSC2 mutation. BMC Cancer. 2018;18(1):561.

3. Iyer G, Hanrahan AJ, Milowsky MI, Al-Ahmadie H, Scott SN, Janakiraman M, et al. Genome sequencing identifies a basis for everolimus sensitivity. Science. 2012;338(6104):221.

4. Maroto P, Anguera G, Roldan-Romero JM, Apellaniz-Ruiz M, Algaba F, Boonman J, et al. Biallelic TSC2 Mutations in a Patient With Chromophobe Renal Cell Carcinoma Showing Extraordinary Response to Temsirolimus. J Natl Compr Canc Netw. 2018;16(4):352-8.

5. Rodriguez-Moreno JF, Apellaniz-Ruiz M, Roldan-Romero JM, Duran I, Beltran L, Montero-Conde C, et al. Exceptional Response to Temsirolimus in a Metastatic Clear Cell Renal Cell Carcinoma With an Early Novel MTOR-Activating Mutation. J Natl Compr Canc Netw. 2017;15(11):1310-5.

6. Wagle N, Grabiner BC, Van Allen EM, Amin-Mansour A, Taylor-Weiner A, Rosenberg M, et al. Response and acquired resistance to everolimus in anaplastic thyroid cancer. N Engl J Med. 2014;371(15):1426-33.

7. Wagle N, Grabiner BC, Van Allen EM, Hodis E, Jacobus S, Supko JG, et al. Activating mTOR mutations in a patient with an extraordinary response on a phase I trial of everolimus and pazopanib. Cancer Discov. 2014;4(5):546-53.

8. Kwiatkowski DJ, Choueiri TK, Fay AP, Rini BI, Thorner AR, de Velasco G, et al. Mutations in TSC1, TSC2, and MTOR Are Associated with Response to Rapalogs in Patients with Metastatic Renal Cell Carcinoma. Clin Cancer Res. 2016;22(10):2445-52.

9. Roldan-Romero JM, Beuselinck B, Santos M, Rodriguez-Moreno JF, Lanillos J, Calsina B, et al. PTEN expression and mutations in TSC1, TSC2 and MTOR are associated with response to rapalogs in patients with renal cell carcinoma. Int J Cancer. 2020;146(5):1435-44.

10. Roldan-Romero JM, Rodriguez-Moreno JF, Garcia-Donas J, Rodriguez-Antona C. mTOR Pathway Mutations and Response to Rapalogs in RCC-Letter. Clin Cancer Res. 2017;23(17):5320.

11. Voss MH, Chen D, Reising A, Marker M, Shi J, Xu J, et al. PTEN Expression, Not Mutation Status in TSC1, TSC2, or mTOR, Correlates with the Outcome on Everolimus in Patients with Renal Cell Carcinoma Treated on the Randomized RECORD-3 Trial. Clin Cancer Res. 2019;25(2):506-14.

12. Voss MH, Hakimi AA, Pham CG, Brannon AR, Chen YB, Cunha LF, et al. Tumor genetic analyses of patients with metastatic renal cell carcinoma and extended benefit from mTOR inhibitor therapy. Clin Cancer Res. 2014;20(7):1955-64.

13. Voss MH, Hsieh JJ. Therapeutic Guide for mTOuRing through the Braided Kidney Cancer Genomic River. Clin Cancer Res. 2016;22(10):2320-2.

14. Roldan-Romero JM, Santos M, Lanillos J, Caleiras E, Anguera G, Maroto P, et al. Molecular characterization of chromophobe renal cell carcinoma reveals mTOR pathway alterations in patients with poor outcome. Mod Pathol. 2020;33(12):2580-90.

15. Wieczorek S, Combes F, Lazar C, Giai Gianetto Q, Gatto L, Dorffer A, et al. DAPAR & ProStaR: software to perform statistical analyses in quantitative discovery proteomics. Bioinformatics. 2017;33(1):135-6.

16. Emsley P, Cowtan K. Coot: model-building tools for molecular graphics. Acta Crystallogr D Biol Crystallogr. 2004;60(Pt 12 Pt 1):2126-32.

17. Schrodinger LLC. The PyMOL Molecular Graphics System, Version 2.0. 2017.

18. Sheen JH, Zoncu R, Kim D, Sabatini DM. Defective regulation of autophagy upon leucine deprivation reveals a targetable liability of human melanoma cells in vitro and in vivo. Cancer Cell. 2011;19(5):613-28.

19. Chen Z, Wang HW, Wang S, Fan L, Feng S, Cai X, et al. USP9X deubiquitinates ALDH1A3 and maintains mesenchymal identity in glioblastoma stem cells. J Clin Invest. 2019;129(5):2043-55.

20. Li J, Li H, Zhu W, Zhou B, Ying J, Wu J, et al. Deubiquitinase inhibitor degrasyn suppresses metastasis by targeting USP5-WT1-E-cadherin signalling pathway in pancreatic ductal adenocarcinoma. J Cell Mol Med. 2020;24(2):1370-82.

21. Luo H, Jing B, Xia Y, Zhang Y, Hu M, Cai H, et al. WP1130 reveals USP24 as a novel target in T-cell acute lymphoblastic leukemia. Cancer Cell Int. 2019;19:56.

22. Udeshi ND, Svinkina T, Mertins P, Kuhn E, Mani DR, Qiao JW, et al. Refined preparation and use of anti-diglycine remnant (K-epsilon-GG) antibody enables routine quantification of 10,000s of ubiquitination sites in single proteomics experiments. Mol Cell Proteomics. 2013;12(3):825-31.

23. Potu H, Peterson LF, Kandarpa M, Pal A, Sun H, Durham A, et al. Usp9x regulates Ets-1 ubiquitination and stability to control NRAS expression and tumorigenicity in melanoma. Nat Commun. 2017;8:14449.

24. Peng H, Yang J, Li G, You Q, Han W, Li T, et al. Ubiquitylation of p62/sequestosome1 activates its autophagy receptor function and controls selective autophagy upon ubiquitin stress. Cell Res. 2017;27(5):657-74.

25. You Z, Jiang WX, Qin LY, Gong Z, Wan W, Li J, et al. Requirement for p62 acetylation in the aggregation of ubiquitylated proteins under nutrient stress. Nat Commun. 2019;10(1):5792.

26. Mimnaugh EG, Xu W, Vos M, Yuan X, Isaacs JS, Bisht KS, et al. Simultaneous inhibition of hsp 90 and the proteasome promotes protein ubiquitination, causes endoplasmic reticulum-derived cytosolic vacuolization, and enhances antitumor activity. Mol Cancer Ther. 2004;3(5):551-66.

27. Wang C, Gao D, Guo K, Kang X, Jiang K, Sun C, et al. Novel synergistic antitumor effects of rapamycin with bortezomib on hepatocellular carcinoma cells and orthotopic tumor model. BMC Cancer. 2012;12:166.

28. Pan JA, Sun Y, Jiang YP, Bott AJ, Jaber N, Dou Z, et al. TRIM21 Ubiquitylates SQSTM1/p62 and Suppresses Protein Sequestration to Regulate Redox Homeostasis. Mol Cell. 2016;61(5):720-33.

29. Mauthe M, Orhon I, Rocchi C, Zhou X, Luhr M, Hijlkema KJ, et al. Chloroquine inhibits autophagic flux by decreasing autophagosome-lysosome fusion. Autophagy. 2018;14(8):1435-55.

30. Runwal G, Stamatakou E, Siddiqi FH, Puri C, Zhu Y, Rubinsztein DC. LC3-positive structures are prominent in autophagy-deficient cells. Sci Rep. 2019;9(1):10147.

31. Dietachmayr M, Rathakrishnan A, Karpiuk O, von Zweydorf F, Engleitner T, Fernandez-Saiz V, et al. Antagonistic activities of CDC14B and CDK1 on USP9X regulate WT1-dependent mitotic transcription and survival. Nat Commun. 2020;11(1):1268.

32. Kodani A, Moyer T, Chen A, Holland A, Walsh CA, Reiter JF. SFI1 promotes centriole duplication by recruiting USP9X to stabilize the microcephaly protein STIL. J Cell Biol. 2019;218(7):2185-97.

33. O'Dea R, Santocanale C. Non-canonical regulation of homologous recombination DNA repair by the USP9X deubiquitylase. J Cell Sci. 2020;133(3).

34. Wang P, Xia J, Zhang L, Zhao S, Li S, Wang H, et al. SNX17 Recruits USP9X to Antagonize MIB1-Mediated Ubiquitination and Degradation of PCM1 during Serum-Starvation-Induced Ciliogenesis. Cells. 2019;8(11).

35. Jia J, Bissa B, Brecht L, Allers L, Choi SW, Gu Y, et al. AMPK, a Regulator of Metabolism and Autophagy, Is Activated by Lysosomal Damage via a Novel Galectin-Directed Ubiquitin Signal Transduction System. Mol Cell. 2020;77(5):951-69 e9.

36. Bailey MH, Tokheim C, Porta-Pardo E, Sengupta S, Bertrand D, Weerasinghe A, et al. Comprehensive Characterization of Cancer Driver Genes and Mutations. Cell. 2018;174(4):1034-5.

37. Kapuria V, Peterson LF, Fang D, Bornmann WG, Talpaz M, Donato NJ. Deubiquitinase inhibition by small-molecule WP1130 triggers aggresome formation and tumor cell apoptosis. Cancer Res. 2010;70(22):9265-76.

38. Driessen S, Berleth N, Friesen O, Loffler AS, Bohler P, Hieke N, et al. Deubiquitinase inhibition by WP1130 leads to ULK1 aggregation and blockade of autophagy. Autophagy. 2015;11(9):1458-70.

39. Fu P, Du F, Liu Y, Yao M, Zhang S, Zheng X, et al. WP1130 increases cisplatin sensitivity through inhibition of usp9x in estrogen receptor-negative breast cancer cells. Am J Transl Res. 2017;9(4):1783-91.

40. Liu H, Chen W, Liang C, Chen BW, Zhi X, Zhang S, et al. WP1130 increases doxorubicin sensitivity in hepatocellular carcinoma cells through usp9x-dependent p53 degradation. Cancer Lett. 2015;361(2):218-25.

41. Ma T, Chen W, Zhi X, Liu H, Zhou Y, Chen BW, et al. USP9X inhibition improves gemcitabine sensitivity in pancreatic cancer by inhibiting autophagy. Cancer Lett. 2018;436:129-38.

42. Bridges CR, Tan MC, Premarathne S, Nanayakkara D, Bellette B, Zencak D, et al. USP9X deubiquitylating enzyme maintains RAPTOR protein levels, mTORC1 signalling and proliferation in neural progenitors. Sci Rep. 2017;7(1):391.

43. Wrobel L, Siddiqi FH, Hill SM, Son SM, Karabiyik C, Kim H, et al. mTORC2 Assembly Is Regulated by USP9X-Mediated Deubiquitination of RICTOR. Cell Rep. 2020;33(13):108564.

44. Savio MG, Wollscheid N, Cavallaro E, Algisi V, Di Fiore PP, Sigismund S, et al. USP9X Controls EGFR Fate by Deubiquitinating the Endocytic Adaptor Eps15. Curr Biol. 2016;26(2):173-83.

45. Lee H, Kim MN, Ryu KY. Effect of p62/SQSTM1 polyubiquitination on its autophagic adaptor function and cellular survival under oxidative stress induced by arsenite. Biochem Biophys Res Commun. 2017;486(3):839-44.

46. Ichimura Y, Waguri S, Sou YS, Kageyama S, Hasegawa J, Ishimura R, et al. Phosphorylation of p62 activates the Keap1-Nrf2 pathway during selective autophagy. Mol Cell. 2013;51(5):618-31.

47. Matsumoto G, Wada K, Okuno M, Kurosawa M, Nukina N. Serine 403 phosphorylation of p62/SQSTM1 regulates selective autophagic clearance of ubiquitinated proteins. Mol Cell. 2011;44(2):279-89.

48. Sanchez-Garrido J, Sancho-Shimizu V, Shenoy AR. Regulated proteolysis of p62/SQSTM1 enables differential control of autophagy and nutrient sensing. Sci Signal. 2018;11(559).

49. Lin Q, Dai Q, Meng H, Sun A, Wei J, Peng K, et al. The HECT E3 ubiquitin ligase NEDD4 interacts with and ubiquitylates SQSTM1 for inclusion body autophagy. J Cell Sci. 2017;130(22):3839-50.

50. Lee Y, Chou TF, Pittman SK, Keith AL, Razani B, Weihl CC. Keap1/Cullin3 Modulates p62/SQSTM1 Activity via UBA Domain Ubiquitination. Cell Rep. 2017;19(1):188-202.

Figures

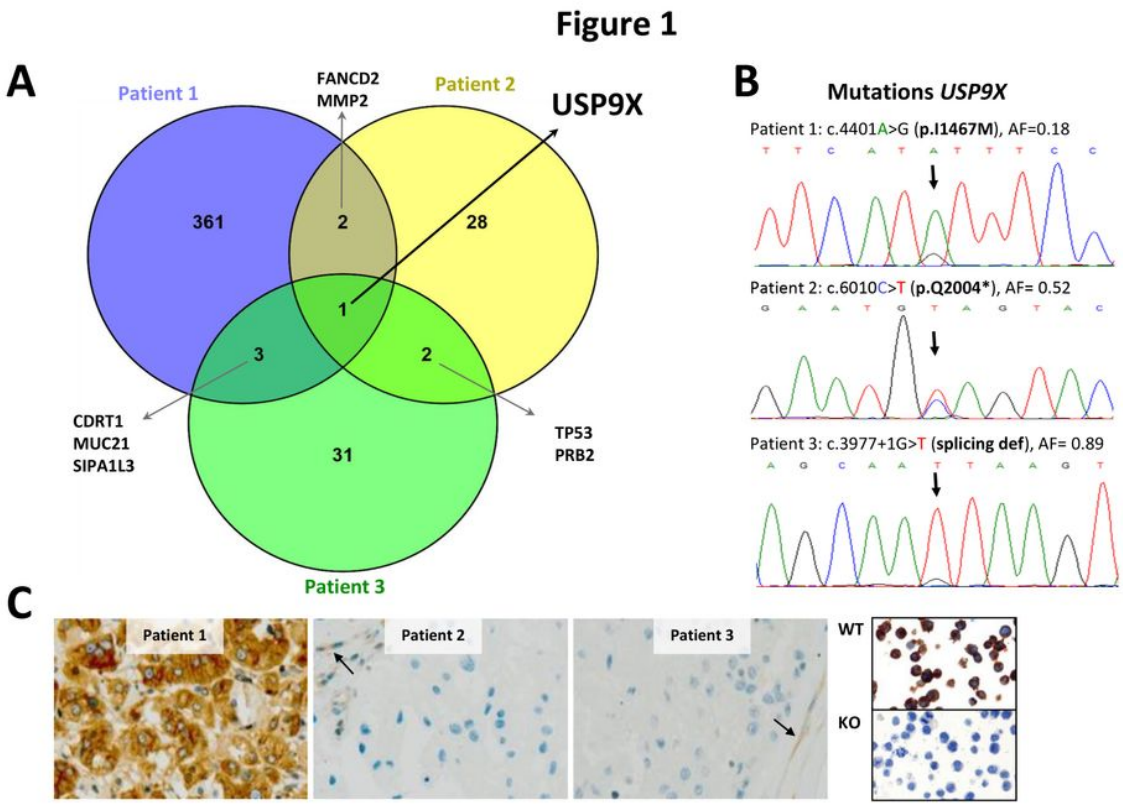

Figure 1

Whole Exome Sequencing revealed USP9X as the only shared mutated gene. (A) Venn diagram showing the number of mutated genes in tumors of the three patients, after germline filtering to retain only tumor-specific alterations. (B) Sanger sequencing chromatograms validating the somatic variants found in USP9X. (C) IHC images for USP9X protein in tumor tissues of the three patients. HAP1 wild type (WT) and HAP1 CRISPR/Cas9 USP9X-KO cell line were used as a control for the IHC.

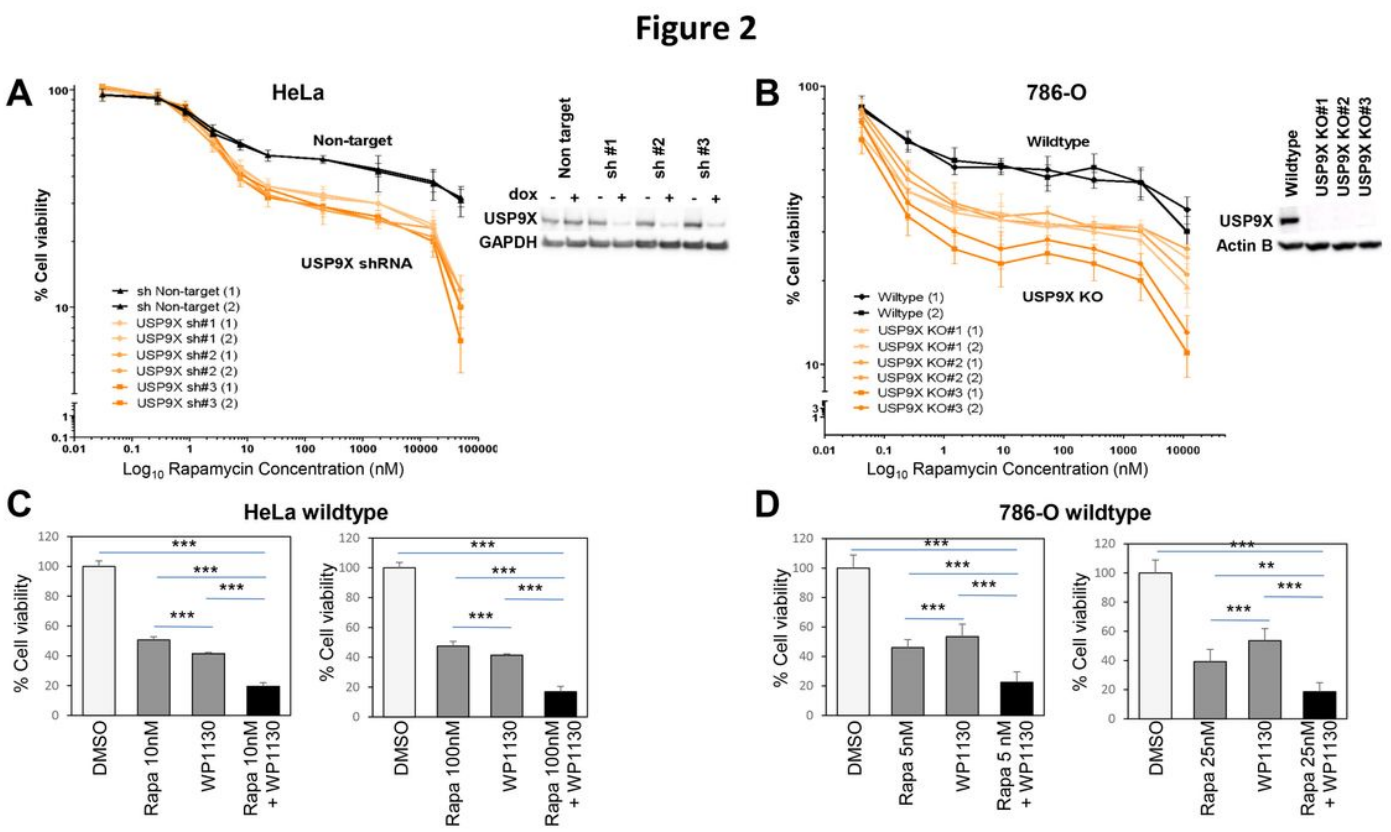

Figure 2

Genetic or chemical USP9X inhibition increases rapamycin sensitivity in HeLa and 786-O cell lines. A) Cell viability assay in HeLa cells expressing doxycycline-inducible shRNA targeting USP9X (sh#1-3) or control shRNA (non-target), together with western blots for USP9X from whole cell protein extracts prepared from HeLa cells expressing doxycycline-inducible shRNAs targeting USP9X. B) Cell viability assay in 786-O cells edited with CRISPR/Cas9 to knock-out USP9X (USP9X KO1, KO2, KO3 clones) or wild type cells, together with western blots for USP9X from whole cell protein extracts prepared from 786-O knockout clones. C) Cell viability in HeLa cells or D) 786-O wild type cells treated with rapamycin (Rapa), the USP9X inhibitor WP1130 (750nM for HeLa and 500nM for 786-O) or a combination of both.

Figure 3

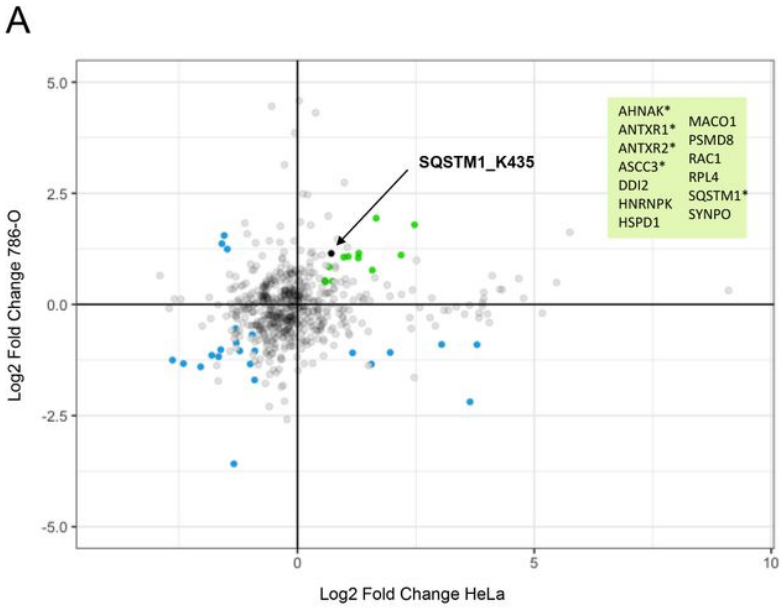

B

SQSTM1 (p62) lysine residues	786-O		HeLa	
	Log2 Fold change	- log10 p-value	Log2 Fold change	- log10 p-value
435	**1.148**	**5.372**	**0.714**	**3.383**
157	1.217	6.416	0.065	0.157
13	0.686	4.818	-0.133	0.315
295	0.035	0.033	0.533	2.774
264	-	-	4.367	10.081
313	-	-	0.746	4.663

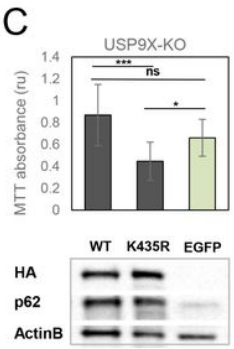

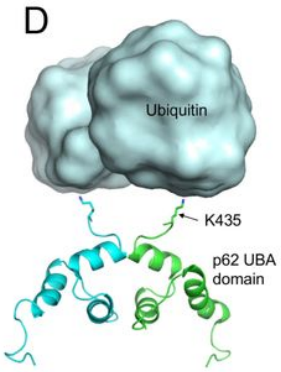

Figure 3

Global ubiquitinome analysis reveals SQSTM1/p62 as a substrate of USP9X. A) Scatter plot graph presenting the enriched-ubiquitinated peptides fold change comparing USP9X depleted versus control cells, in HeLa and 786-O models. Ubiquitinated peptides upregulated in both models with a log2-fold change ≥0.5 and p-values≤0.001 in both models (n=13) are colored in green and SQSTM1 K435 residue is marked in black. Additional significantly regulated residues are colored in blue. In the protein list, those with several ubiquitinated residues in HeLa or 786-O are marked with an asterisk. B) List of SQSTM1/p62 ubiquitinated peptides detected with a log2 FC>0.5 and p-value <0.001 in the two cell models. Values fulfilling these criteria in both cell models are in bold. C) USP9X KO cells were transiently transfected with p62-wild type and p62-K435R constructs and cell viability was assessed using an MTT assay 58h after transfection in two different USP9X-KO clones. Bars represent mean and standard deviation values (***p <0.0001). Control cells were transfected with an EGFP expression plasmid. D) Structural model of p62-UBA dimer and ubiquitin. The p62-UBA domain dimer is shown as cartoon representation and the side chain of K435 in p62-UBA is shown as sticks. The surface of two ubiquitin molecules is shown in blue.

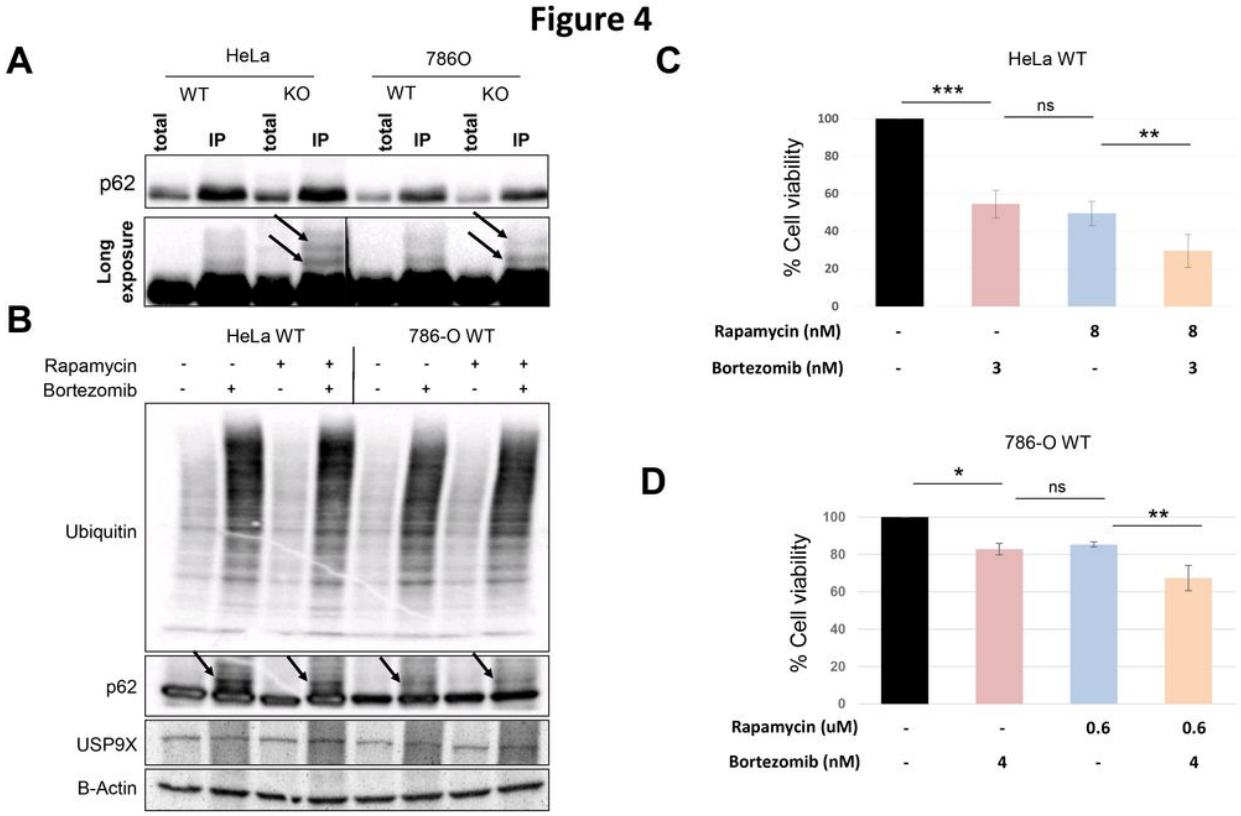

Figure 4

Ubiquitinated p62 accumulation in USP9X depleted cells and bortezomib treated cells exhibiting increased rapamycin sensitivity. A) Western blot of p62 immunoprecipitated proteins in USP9X depleted and wild type (WT) cells, revealed higher p62 molecular weight bands in KO cells. B) Bortezomib treatment (3nM) and/or rapamycin (1μM) in HeLa (24h) and 786-O (20h) wildtype cells promoted global accumulation of ubiquitin conjugates. Arrows indicate higher molecular weight bands. Rapamycin sensitivity is increased by bortezomib treatment in C) HeLa (3nM for 72h) and D) 786-O (4nM for 48h) wild type cells. P-values correspond to Mann-Whitney U test comparing the combination of rapamycin and bortezomib treatment versus each of the drugs alone (* $p<0.05$, ** $p<0.01$, ***$p<0.001$).

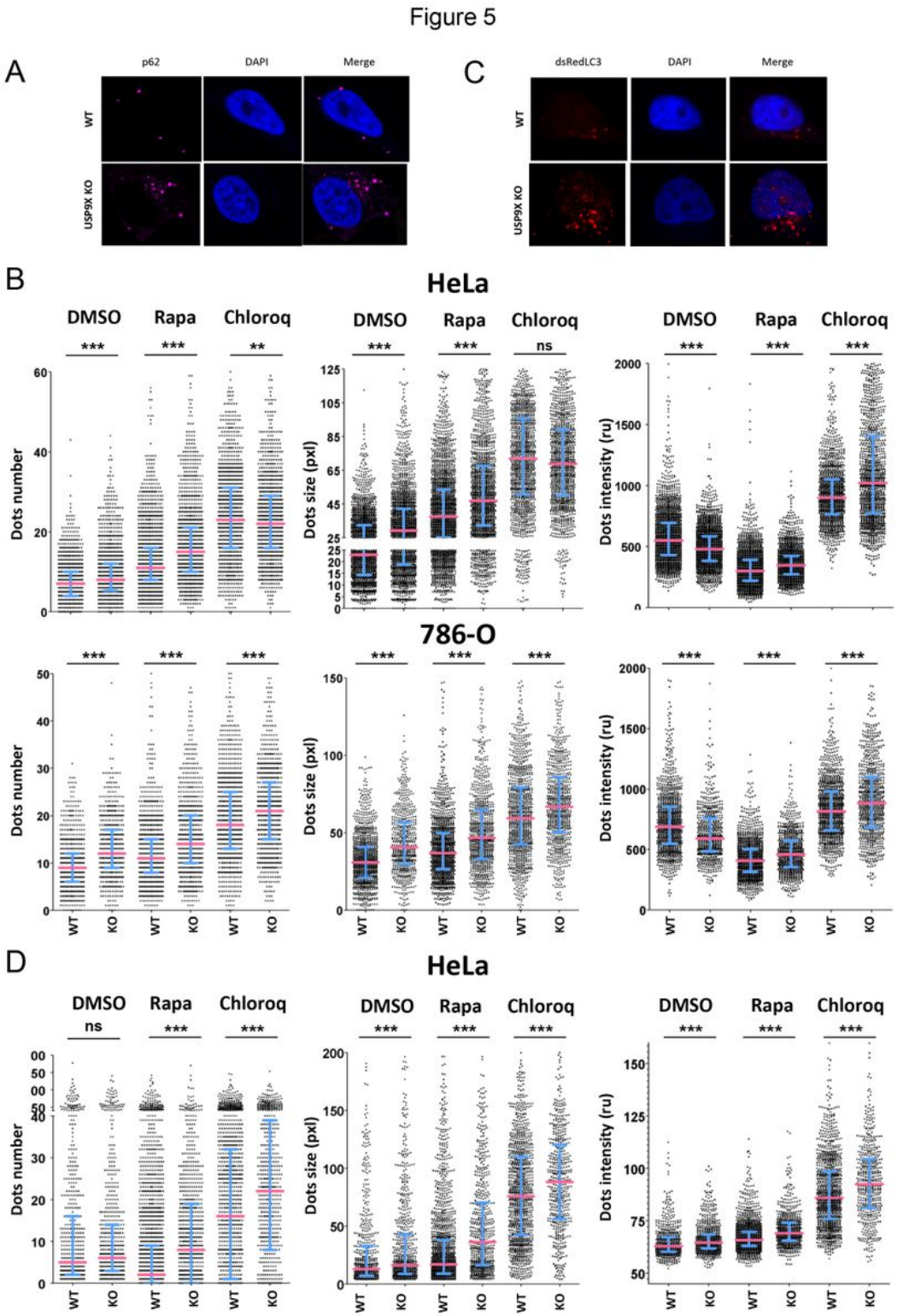

Figure 5

Immunofluorescence of p62 and dsRed-LC3 expression in HeLa and 786-O cell models. A) Representative p62 immunofluorescence images in USP9X depleted and wild type HeLa cells. B) p62 immunofluorescence quantification in USP9X depleted and wildtype HeLa and 786-O cells under normal conditions, rapamycin (5uM or 10uM) and chloroquine (30uM) treatment. C) Representative dsRed-LC3 immunofluorescence images in USP9X depleted and wild type HeLa cells. D) dsRed-LC3 expression

quantification in wildtype and knock-out HeLa cells under normal conditions, rapamycin (5uM) and chloroquine (30uM) treatment. P-values correspond to Mann-Whitney U test (* p<0.05, ** p<0.01, ***p<0.001). Rapa (rapamycin), Chloroq (chloroquine), Wildtype (WT).

Supplementary Files

This is a list of supplementary files associated with this preprint. Click to download.

- SupplementaryTable1.MutationsWESalltumors.xlsx
- TextUSP9XRoldanRomeroSUPPLINFORMATION.docx
- renamed0e3f1.xlsx